An example of consistent palaeostress regime resulting in morphometric irregularity in the northwestern part of Noachis Terra, Mars

The Noachis Terra, a vast Martian terrain situated between the Tharsis province to the west and the gigantic impact basin of Hellas to the east in the southern hemisphere of the planet, preserves numerous geomorphic features like wrinkle ridges, lobate scarps, grabens, drainage channels, dunes, etc. Though the morphotectonic features of Mars have been a subject of interest for geologists for the last four decades[1–4], little is known about the Noachis Terra[5–7]. Rendering the geologic evolution of the Terra unexplained till date, we attempt to document a set of morphotectonic features of the Terra in this study and aim to resolve the palaeostress condition that led to its development. The conspicuous E–W trending grabens present in the Middle Noachian Highland unit[8] in the western part (26°W, 26°S to 19°W, 32°S) of the Noachis Terra are used in this study. MOLA[9] Digital Terrain Model (DTM) and high resolution optical (HRSC and CTX)[10,11] images are used as datasets. Profiles, based on MOLA DTM, are drawn to elucidate the topography/structure, while HRSC and CTX images are used for clear observations of the topographic features[12].

Available data are insufficient to constrain the actual dip of the fault planes present in the Martian crust. The scarps on the Martian surface commonly show very shallow dip[13] (~9°); however, knowledge on inclination of faults in basalts and other volcanics at the shallow crustal levels[14,15] and also the comparatively lesser gravity on Mars than the Earth[16] led geologists to consider emergent extensional faults on Mars as steeply (60–80°) dipping surfaces[13,17,18]. Fault plane orientations and slip data aid in the determination of the states of palaeostress responsible for the formation of faults[19–21]. Geologists have extended the application of this technique for faults on the Martian surface to unveil the stress conditions that prevailed in areologic past[22]. In the present work the fault plane orientations and slip directions along the fault planes were analysed using T-Tecto 3.0 (ref. 23) software to understand the palaeostress regime in which the faults were formed.

MOLA DTM reveals a system of subparallel grabens (Figure 1 *a*), all of which trend almost E–W. Such a regularity in orientation spread over an area of 140,800 sq. km hints to a somewhat consistent internal stress regime responsible for development of faults that limit the grabens[18,24]. The lengths of the traces of these lineaments vary from ~20 to ~120 km. An unnamed crater (addressed as CR hereafter), to the east of the Sangar crater (24.3°W, 27.5°S) and south of Pabo crater (23.1°W, 26.9°S; Figure 1 *a*) is transected by the northernmost graben (F_A). CR has an almost circular rim, the northeastern part of which is faint possibly due to prolonged weathering and erosion. NE–SW trending wind streaks[25] and a seemingly drainage channel trending roughly north–south is present within the northern part of the crater (Figure 1 *b*). Therefore, the crater floor must be covered by sediments which hinder the measurement of elevation of the actual floor of the crater. Low (0.005) depth-to-diameter ratio[26] and presence of sharp rim crest at parts, rules out the possibility of considering CR as a volcanic caldera and indicates its impact origin[27]. F_A is ~93 km long. Profile section reveals two scarps (Figure 1 *c*), the northern one dipping south and the southern one dipping north, bordering the graben, the floor of which shows a drop-down of ~150–200 m from the adjacent ground level along its strike. However, this drop-down is not the actual throw of the faults as the surface must be covered by sediments. The ground level outside CR to the north of F_A graben is lower than (20–50 m along F_A) that to the south of F_A (Figure 1 *a*, *c* and *d*). This fact can be attributed to a composite effect of relatively lesser displacement along the northern fault of F_A and a possible difference in the degree of weathering and erosion across the graben as evident from fluvial and aeolian activity seen in the region (Figure 2 *a*). The CR rim shows no visible offset along F_A lineament, as found from high-resolution HRSC image (Figure 1 *b*). Such a condition can only be explained if the concerned faults bordering F_A are dip slip faults (Figure 1 *d*). Profile sections (Figure 2 *b*, *c*) reveal seven more ~E–W trending grabens (F_C, F_E, F_I, F_K, F_L, F_M and F_N; Figure 1 *a*). Another graben (F_D) to the west of F_A may be a segment of extension of F_A to the west along its strike, as it coincides with F_D (Figure 1 *a*). The graben floors have ~20–170 m drop relative to the ground level outside them. In all the grabens, inclinations of the bordering scarps face each other revealing that the depression is due to relative downward movement of the hanging wall of the bordering normal faults[28]. Graben F_B is possibly a continuation of graben F_C. The F_E, F_J, F_G and F_H (Figure 1 *a*) may be segments of a single graben, presently discontinuous due to partial obliterations by impact craters and possibly due to buried nature. The regional structure is therefore a series of grabens (Figure 2 *b*, *c*).

The region is one of the oldest terranes on the Martian crust[29] and therefore must have undergone prolonged action of surface geological processes. The study area has a northward regional slope resulting in 500 m drop in elevation from southern to northern extremity (Figure 2 *b*, *c*). Erosional activity in addition to faulting might have played a role in this large difference in elevation.

A drainage channel appears to have originated from the Pabo crater on the northernmost point of the CR rim. This channel runs N–S on the CR floor up to F_A and takes an eastward turn along it and again runs southward outside CR[8]. However, observations using MOLA DTM show that the channel floor to the north of the graben has a southward slope and that on the south has a northward slope, indicating that these are two different channels. The channels postdate F_A as both terminate at the fracture and are not extended beyond it. Other drainage channels radiate from the flanks of craters (Figure 1 *a*) and some of them have ~SSW to NNE slope. Structural lineaments could have guided these channels. There are no perceptible differences of the ground level across these channels (Figure 2 *d* and *e*) as well as no offset of other linear features indicating to extensional fracturing without considerable

shear. These channels do not cross-cut any of the E–W trending scarps, indicating that the channels and also the lineaments postdate the E–W scarps.

For fault-slip analysis in order to understand the palaeostress scenario trends of small segments of the faults along their traces are used to estimate all possible variations in the strike and the corresponding dip directions. Guided by the steepness of the Martian extensional faults, fault-plane dips are considered as 60–80° (cf. ref. 18), except for vertical faults of F_A. In the absence of any offset of linear surface features along the faults and also of any data on displaced marker horizons, the faults are considered as dip-slip faults, i.e. with high values (80–90°) of rakes for the slip-lines. The faults and the corresponding slip directions are projected stereographically (Figure 2 *f*) using T-Tecto 3.0. The slip vector analysis (cf. refs 18, 22 and 23) of the set of these faults bounding the grabens reveals a subvertical maximum principal stress (σ_1), and a N–S trending sub-horizontal minimum principal stress (σ_3) direction (Figure 2 *f*).

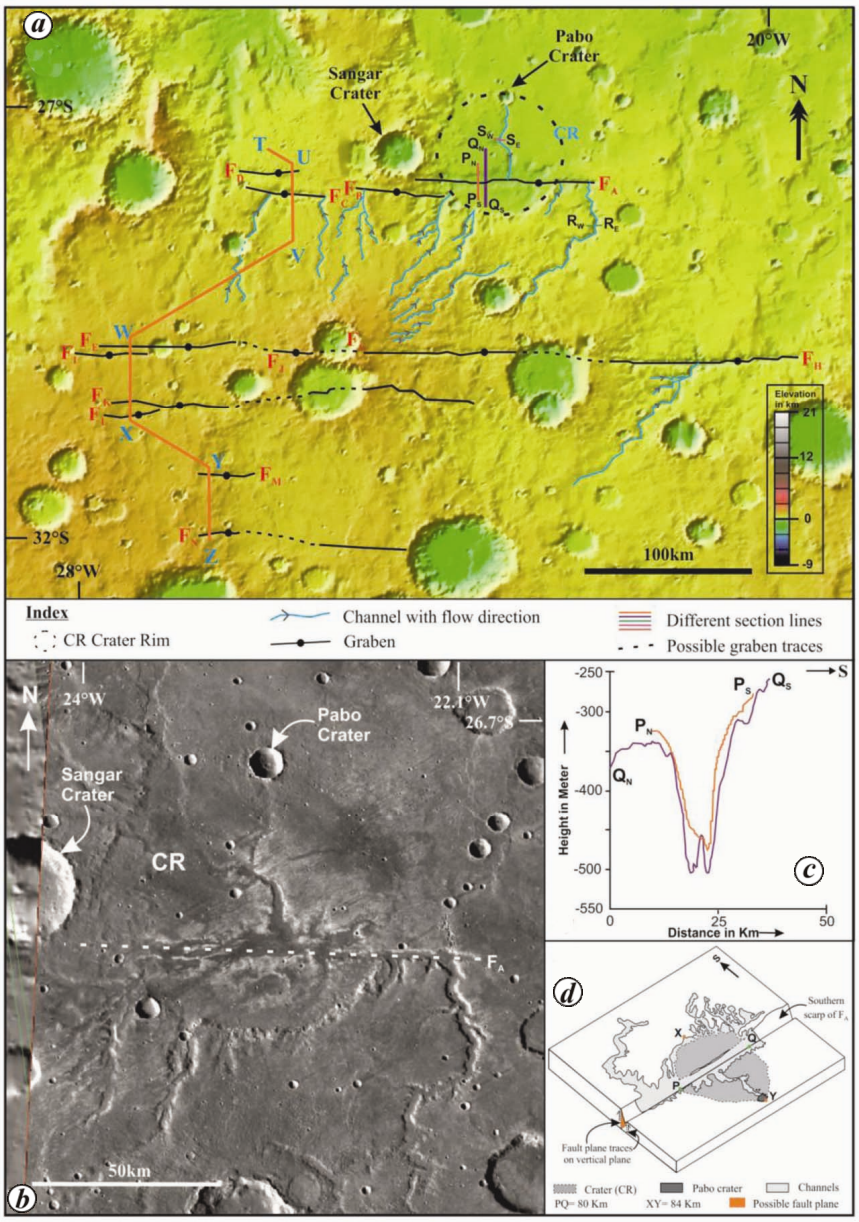

Figure 1. ***a***, Grabens shown (F_A, F_B, F_C, F_D, F_E, F_G, F_H, F_I, F_J, F_K, F_L, F_M and F_N) on MOLA DTM of the area of study. P_N–P_S and Q_N–Q_S are section-lines (profiles shown (***c***)) across the F_A fracture that intersects the unnamed crater (CR). *T*–*Z* is the line of section used for deriving the topographic profile (in (***b***)) of the area avoiding the craters. On the *T*–*Z* line *U*, *V*, *W*, *X*, *Y* are points where the section line is bent. R_W–R_E and S_W–S_E are the section lines across two N–S trending channels. Also note the radial pattern of channels emerging from the flank of slope of a large crater. ***b***, HRSC image (H9319_0000_ND3) showing absence of any offset of the rim of CR along the graben (F_A). ***c***, Profile sections across the F_A graben. See (*a*) for the section-lines (P_N–P_S and Q_N–Q_S). ***d***, Schematic representation of the structure across the limiting scarps of the F_A graben. Graben width and depth are given in Table 1.

The region is situated between two important tectonic provinces, the volcano-tectonic Tharsis province in the west and the gigantic impact basin of Hellas Planitia in the east. Tharsis has a long history of tectonic evolution spanning between Early Noachian and Amazoinian periods[30], whereas age of the Hellas impact is Early Noachian[24]. The centre of another large impact basin, the Argyre Planitia, of early (?) to Mid Noachian age[24] is ~1400 km SW of the area. The grabens and faults studied here are superposed by large impact craters (Figure 1 *a*), which must postdate the grabens. It is known that large impacts happened in the early history of the planet[31] and therefore, it is evident that the grabens were formed in the early times of the planet Mars. Grabens of similar trends are present in the Thaumasia Planum[4,32], ~2000 km away, within the Tharsis province, which do not continue to the present study area. Therefore, though of similar trends, grabens of these two regions cannot be directly correlated. Faults with similar geometry are absent in the vicinities of both Argyre and Hellas basins, opposing any possible correlation between the origin of the present grabens and the impact events. Tharsis tectonism and Hellas impact deformed the crust on a global scale[24,30] and their roles in the extensional deformation of the western part of Noachis Terra cannot be fully ruled out, although any direct link to establish the relation is still undiscovered.

There are differing opinions on graben formation on the Martian surface; some of them advocate emplacement of dykes[33] and some favour tectonic extension[18]. The grabens in this area are smaller in terms of width and depth compared to large rift systems of Mars. Wilson and Head[24] have suggested ranges of values of width and depths of grabens that are generated by dyke emplacements. The depths and widths of the presently studied grabens (Table 1) are well within this specified range. Korteniemi *et al.*[33] have suggested

Table 1. Depth of floor and width of the grabens

Graben	F_A	F_C	F_D	F_E	F_I	F_K	F_L	F_M	F_N
Depth of graben floor (m)	150	170	40	45	60	20	30	25	90
Width (km)	13	8	8	3	5	3	3	3	6

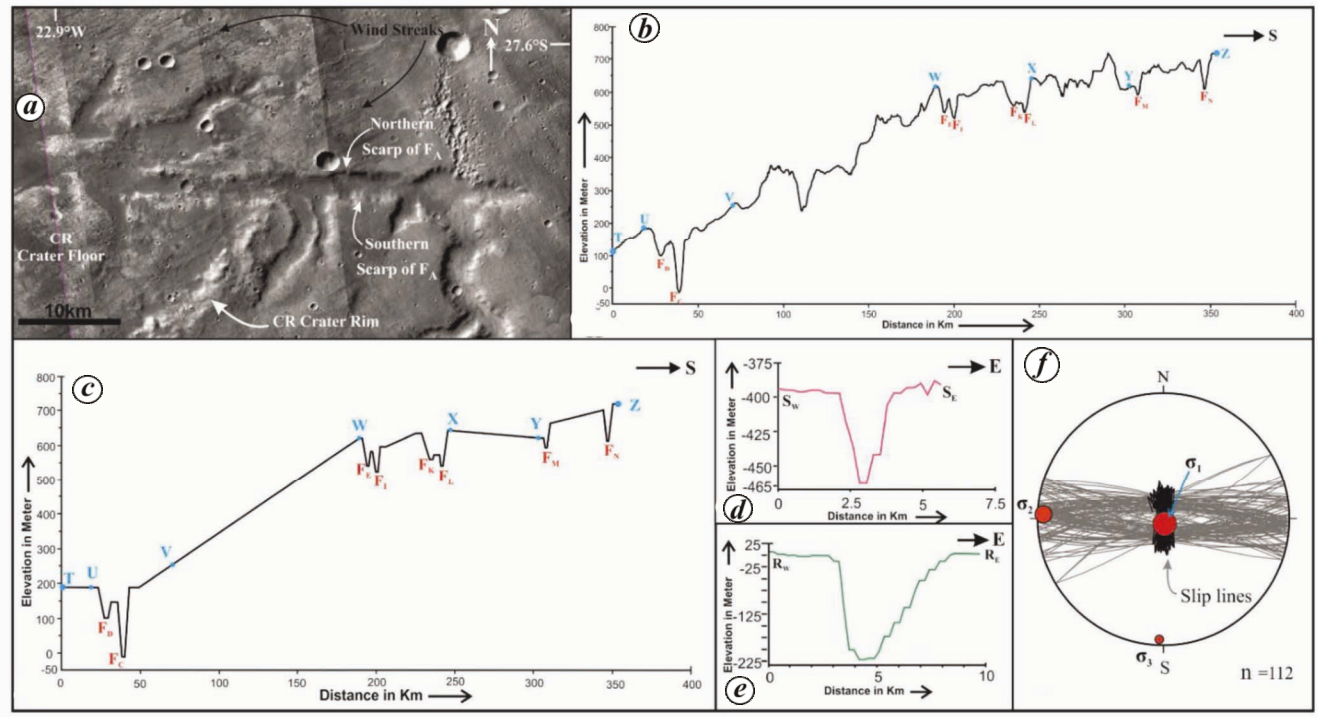

Figure 2. ***a***, Mosaic of CTX (P08_004237_1506_XI_29S023W, D20_034934_1520_XN_28S022W, B17_016381_1524_XN_27S022W) and HRSC (H9319_0000_ND3) showing a portion of the CR crater and the F_A graben. Note presence of channels and wind streaks.. ***b***, Profile section along the *T*–*Z* line in the section showing the grabens (F_D, F_C, F_E, F_I, F_K, F_L, F_M, F_N). Widths of grabens and depths of graben floors are presented in Table 1. Points of bend along the section-line are marked (*U*, *V*, *W*, *X*, *Y*; see (***a***)). ***c***, Structural interpretation of the geomorphic features presented in (***b***). Note presence of grabens, marked by F_D, F_C, F_E, F_I, F_K, F_L, F_M, F_N from north to south. ***d***, Profile section along S_W–S_E (***a***) showing no significant difference in elevation of the ground across the N–S channel initiating from Pabo crater. ***e***, Profile section along R_W–R_E showing no significant elevation change across S–N trending channel. ***f***, Stereographic projection of fault planes and slips along the fault planes limiting each of the grabens (F_A, F_B, F_C, F_D, F_E, F_G, F_H, F_I, F_J, F_K, F_L, F_M, F_N). The projection reveals vertical maximum principal stress (σ_1) and N–S trending minimum principal stress (σ_3).

that dykes extending from north and west of Hellas basin to the Argyre Planitia are present beneath the Noachis Terra. Therefore, available information and the data generated on morphology of the present grabens indicate emplacement of dykes generating subvertical principal compressive stress that has caused subsidence along steeply dipping normal faults. To summarize, the area experienced normal faulting under a stress regime consisting of subvertical maximum compressive stress and N–S trending maximum subhorizontal extension resulting in a series of E–W trending grabens. The palaeostress regime cannot be linked either to Tharsis tectonism or to the Hellas and Argyre impacts. However, emplacement of dykes generating a vertical maximum principal stress and corresponding horizontal extension can be envisaged for formation of the normal fault-bound grabens.

1. Montgomery, D. R., Som, S. M., Jackson, M. P. A., Schreiber, B. C., Gillespie, A. R. and Adams, J. B., *Geol. Soc. Am. Bull.*, 2009, **121**, 117–133.
2. Golombek, M. P., Franklin, B. J., Tanaka, K. L. and Dohm, J. M., In Proceedings of the Lunar and Planetary Science Conference, 1997, vol. 28, p. 431.
3. Borraccini, F., Di Achille, G., Ori, G. G. and Wezel, F. C., *J. Geophys. Res.*, 2007, **112**, E05005; doi: 10.1029/2006-JE002866.
4. Kundu, A., Ruj, T. and Dasgupta, N., In Proceedings of the Lunar and Planetary Science Conference, 2014, vol. 46, p. 1307.
5. Aittola, M., Korteniemi, J., Öhman, T., Törmänen, T. and Raitala, J., In Proceedings of the Lunar and Planetary Science Conference, 2006, vol. 38, p. 1654.
6. Korteniemi, J., Aittola, M., Öhman, T., Törmänen, T. and Raitala, J., In 42nd Vernadsky–Brown Microsymposium on Comparative Planetology, Moscow, Russia, 2005.
7. Raitala, J., Aittola, M., Korteniemi, J., Öhman, T. and Törmänen, T., In 50th Vernadsky–Brown Microsymposium on Comparative Planetology, Moscow, Russia, 2009.
8. Tanaka, K. L. *et al.*, US Geological Survey 160 Scientific Investigations Map 3292, scale 1:20,000,000, pamphlet 2014, p. 43; http://dx.doi.org/10.3133/sim3292.

9. Smith, D., Neumann, G., Arvidson, R. E., Guinness, E. A. and Slavney, S., Report, NASA Planetary Data System, MGS-M-MOLA-5-MEGDR-L3-V1.0, 2003.
10. Neukum, G., Jaumann, R. and the HRSC Co-Investigator and Experiment Team, In *Mars Express: The Scientific Payload*, (ed. Wilson, A., scientific contribution: Chicarro, A.), European Space Agency Special Publication, SP-1240, Noordwijk, The Netherlands, 2004, pp. 17–35.
11. Malin, M. C. *et al.*, *J. Geophys. Res.*, 2007, **112**, E05S04; doi: 10.1029/2006-JE002808.
12. Christensen, P. R., JMARS – a planetary GIS; http://adsabs.harvard.edu/abs/2009AGUFMIM 22A.06.
13. Golombek, M. P., Tanaka, K. L. and Franklin, B. J., *J. Geophys. Res.*, 1996, **101**, 26119–26130.
14. Day, W. C., Dickerson, R. P., Potter, C. J., Sweetkind, D. S., San Juan, C. A., Drake II, R. M. and Fridrich, C. J., US Geological Survey Miscellaneous Investigations Series Map I-2627, Scale 1 : 24,000, 1998.
15. Dauteuil, O., Huchon, P., Quemeneur, F. and Souriot, T., *Tectonophysics*, 2001, **332**, 423–442.
16. Esposito, P. B. *et al.*, In *Mars* (eds Kieffer, H. H. *et al.*), The University of Arizona Press, USA, 1992, pp. 209–248.
17. Hauber, E. and Kronberg, P., *J. Geophys. Res.*, 2005, **110**, doi: 10.1029/2005-JE002407.
18. Ferrill, D. A., Wyrick, D. Y., Morris, A. P., Sims, D. W. and Franklin, N. M., *GSA Today*, 2004, **14**, 10; doi: 10.1130/1052-5173(2004)014<4:DFSAPC>2.0.CO;2.
19. Mamtani, M. A., Ghosh, A., Chaudhuri, A. K. and Sengupta, D., *Gondwana Res.*, 2003, **7**(2), 579–583.
20. Lee, J.-C., Lu, C.-Y., Chu, H.-T., Delcaillau, B., Angelier, J. and Dettontaines, B., *Terr. Atmos. Ocean. Sci.*, 1996, **7**(4), 431–446.
21. Kaymakci, N., *J. Asian Earth Sci.*, 2006, **27**, 207–222.
22. Wyrick, D., Ferrill, D. A., Morris, A. P., Colton, S. L. and Sims, D. W., *J. Geophys. Res.*, 2004, **109**, E06005; doi: 10.1029/2004JE002240.
23. Žalohar, J., T-TECTO 3.0 Professional. Integrated software for structural analysis of fault-slip data, Department of Geology, University of Ljubljana, SI-1000 Ljubljana, Slovenia, 2009.
24. Wilson, L. and Head III, J. W., *J. Geophys. Res.*, 2002, **107**(E8); doi: 10.1029/2001JE001593.
25. Quintana, S. N. and Schultz, P. H., In Proceedings of the Lunar and Planetary Science Conference, 2014, vol. 45, p. 1971.
26. Barlow, N. G., *LPI Techn. Rep.*, 1993, 93–06, Part-1.
27. Basilevsky, A. T. and Ivanov, B. A., *Geophys. Res. Lett.*, 1990, **17**(2), 175–178.
28. Twiss, R. J. and Moores, E. M., *Structural Geology*, W. H. Freeman and Company, New York, 2nd edn, 2007, p. 736.
29. Fassett, C. I., James W. and Head, J. W., *Icarus*, 2011, **211**, 1204–1214; doi: 10.1016/j.icarus.2010.11.014.
30. Yin, A., *Lithosphere*, 2012, **4**(6), 553–593.
31. Golombek, M. P. and Phillips, R. J., In *Planetary Tectonics* (eds Watters, T. R. and Schultz, R. A.), Cambridge University Press, New York, 2010, pp. 183–232.
32. Vaz, D. A., *Planet. Space Sci.*, 2011, **59**, 1210–1221.
33. Korteniemi, J., Aittola, M., Öhman, T. and Raitala, J., In Proceedings, 40th ESLAB – First International Conference on Impact Cratering in the Solar System (ed. Wilson, A.), ESA Special Publication, 2006, SP-612, pp. 193–198.

ACKNOWLEDGEMENTS. We thank the Space Applications Centre (ISRO), Ahmedabad for a project grant and the Principal, Asutosh College, Kolkata for support.

Received 1 December 2014; revised accepted 1 April 2015

KEYUR DE[1,*]
ABHIK KUNDU[1]
PRAKASH CHAUHAN[2]
NILANJAN DASGUPTA[3]

[1]*Department of Geology, Asutosh College, 92 S.P. Mukherjee Road, Kolkata 700 026, India*
[2]*Space Applications Centre (ISRO), Jodhpur Tekra, Satellite Road, Ahmedabad 380 015, India*
[3]*Department of Geology, Presidency University, 86/1 College Street, Kolkata 700 073, India*
**For correspondence.*
e-mail: de.keyur@gmail.com

Highly potassic melagranite of Bintang Batholith, Main Range Granite, Peninsular Malaysia

For decades, the Main Range Granite Province of Peninsular Malaysia has been regarded to comprise exclusively of S-type granites[1] (T. C. Liew, unpublished), which have been taken as the world standard for collisional *S*-type granite[2]. The Main Range Granite Province is believed to have formed during Triassic[3] continental collision between Sibumasu and Indochina[4] blocks subsequent to the closure of Palaeo-tethys Ocean in Early Permian. However, recently Ghani and coworkers[5,6] have found that the province also contains granites with *I*-type characteristics such as absence of Al-rich minerals such as sillimanite, cordierite, primary wedge titanite and pale green amphibole, occurrence of mafic, hornblende–clinopyroxene–orthopyroxene-bearing enclaves and increasing peraluminosity towards the most differentiated rocks.

The Malaysian Granite Province is primarily made up of two major batholiths, the Main Range batholith and the Bintang batholith (Figure 1). The Granite Province can be divided into four main facies: (i) biotite granite, (ii) amphibole-bearing granite, (iii) subvolcanic and volcanic ± dacite and orthopyroxene rhyodacite, and (4) microgranite and mesogranite associated with aplopegmatite[6]. Biotite granites are present in both batholiths, but amphibole-bearing granites are more common in Bintang batholith. *I*-type character of the Main Range Granite Province is mainly contributed by the amphibole-bearing granite. Our recent and ongoing study on the amphibole-bearing granite in Bintang batholith revealed some interesting petrographical and geochemical features present in the province, as reported in this paper.

The Bintang batholith is located in the northern part of the Main Range Granite Province, forms a N–S elongate-shaped